Supporting Online Material for

Critical Population Density Triggers Rapid Formation of Vast Oceanic Fish Shoals

Nicholas C. Makris,* Purnima Ratilal, Srinivasan Jagannathan, Zheng Gong, Mark Andrews, Ioannis Bertsatos, Olav Rune Godø, Redwood W. Nero, J. Michael Jech

*To whom correspondence should be addressed. E-mail: makris@mit.edu

This PDF file includes

Materials and Methods
Figs. S1 to S6
References

Other Supporting Online Material for this manuscript includes the following:
(available at www.sciencemag.org/cgi/content/full/323/5922/1734/DC1)

Movie S1

Materials and Methods

The overall process of rapid shoal formation, triggered by attainment of a critical density of 0.2 fish/m^2 near sunset, followed by migration towards spawning grounds, is found to describe a regular diurnal pattern. The pattern was observed on 7 of 7 days in the central region of Georges Bank's northern flank during the herring spawning period, and defined the dominant behavior observed there. In this central region, of the highest historical spawning populations (Fig 4E), OAWRS sampling of the shoal formation process was relatively complete on 5 days, September 28, 29, October 1-3, and fragmentary on 2 days, September 30, Oct 5, due to severe autumn weather or logistical constraints at sea. The diurnal shoal formation pattern was also observed by OAWRS at the south western end of Georges Bank's northern flank on September 26, 27, but mixed with apparent eastward migrations of preexisting shoals in the daytime and at night. Later observations at this southwestern extremity on October 4 revealed little activity, suggesting the herring observed there earlier had migrated eastwards.

Documentation of the shoal formation process for the 5 days in the central region of Georges Bank's northern flank when OAWRS sampling was relatively complete appears in Figs 1-4 of the main text for October 3 and September 29, Figs S1-S4 for September 28-29 and October 1-2, and Movie S1 for October 3. Shoal forming convergence waves, traveling at speeds much greater than herring groups swim, consistently appeared near sunset when a critical density of 0.2 fish/m^2 was attained. This was followed by much slower southern migrations consistent with herring group swimming speeds, as shown in Fig 3 and Fig S1-S4. The waves originated within favored bathymetric contours (160-190 m) from small catalyzing clusters, which acted as sources, and tended to propagate along these contours. This led to the formation of large shoals which often extended for tens of kilometers along the northern flank of Georges Bank as shown in Figs 1, 4, S1-S4. The observed shoal forming waves arose from sequences of local synchronous convergence actions and reactions by members of the shoal, which define propagating compressional waves in a medium of variable density (*S1*). Such waves have been theoretically predicted to exist in large animal groups (*S2*). Compressional waves in fish shoals require the propagation of changes in population density and so are inherently different from turning waves (*S3*) which only require the propagation of changes in fish orientation. Our observations show that a small group of leaders initiated shoal formation. Since migration typically occurred sometime after the shoals had already developed, it is not clear that the same leaders responsible for shoal initiation were also responsible for choosing a migration direction. The fact that all migrations were directed towards the spawning ground, however, indicates that the shoal migration directions were not random but were strongly influenced by synchronous spawning behavior.

Population density versus time as shown in Figs 3B-C, S1D-F, S2D, S3B, S4D-E, is the spatial average over a 0.6 km by 0.6 km patch around the region where the shoal initiates in OAWRS imagery. The two solid lines in these figures, whose slopes indicate the rate of change of population density before and after the transition, are the linear least square fits to data points they span. The slopes before a critical density of 0.2 fish/m^2 is attained are consistently orders of magnitude smaller than those after it is attained. Intersection of these least square lines before and after the transition consistently occurs at 0.2 fish/m^2 when rounded to the nearest tenth. The shoal lengths of Figs 3A, S1C, S2C, S3A, S4C, were determined from OAWRS imagery by finding the major axis extent of population density features exceeding 0.2 fish/m^2. The migration distances of southern shoal edges were determined by segmenting the shoal edges with a 0.2 fish/m^2 threshold and estimating the mean location of this edge for a given shoal from OAWRS imagery. The lines shown for shoals lengths during formation and migration distances are linear least square fits to the data points of corresponding color.

Our autumn 2006 OAWRS experiment in the Gulf of Maine and Georges Bank employed four research vessels, the RV Oceanus which towed the OAWRS receiving array and collected OAWRS data, the RV Endeavor from which the OAWRS source array was deployed in either moored or drift mode, the RV Hugh Sharp which collected CFFS data, and the RV Delaware II which collected CFFS and trawl data. The RV Delaware II also conducted the National Marine Fisheries Service Annual Fall Herring Survey

with traditional methods for measuring the distribution, abundance and behavior of oceanic fish populations (*S4-S7*). The beamwidth of the CFFS used by RV Hugh Sharp in our field experiment was 7.0° at 38 kHz, which yields a 20 m diameter resolution footprint at 160-m depth where many of the fish groups we imaged were concentrated, while that for the RV Delaware II was 12.0° at 38 kHz (Fig 2A-B) which leads to a 33 m diameter resolution footprint at 160-m depth.

We used the same OAWRS imaging system described in Ref (*S8*) for all OAWRS measurements presented here, which are the scattered returns of linear frequency modulated (LFM) source waveform transmissions of 50 Hz bandwidth and 1 second duration centered at 950 Hz. Scattered returns at the receiver were beamformed and match filtered leading to a range resolution of 15 m. OAWRS azimuthal resolution in radians varies as the acoustic wavelength λ (1.55 m) divided by the projected array length $L\cos\theta$, where L is the full array length (47.25 m) and the azimuth angle θ is zero at *broadside*, which is normal to the array axis. While 1 second transmissions were sent every 75 seconds at various non-overlapping frequencies to enable imaging over a 100 km diameter, consecutive LFM transmissions centered at 950 Hz were typically sent only every 150 seconds. All OAWRS images presented here are the averaged returns of 3 consecutive 950 Hz LFM transmissions and two consecutive 15-m range cells to obtain intensity averaged with at least 6 independent samples at each pixel of 30-m dimension. Scattering strength (*S9*) was obtained by correcting the measured beamformed and match filtered pressure level for transmitted level, array beampattern and two-way transmission loss (*S10*, *S11*) which was determined by parabolic equation modeling (*S8*, *S11*). OAWRS incident signals were at least 3 orders of magnitude less intense than those of the CFFS. Population density was estimated from scattering strength by determining the mean fish scattering cross section at the OAWRS frequency necessary for OAWRS and CFFS population densities to match over regions where simultaneous measurements of statistically stationary fish populations were available (*S8*).

An example of the measured pressure level of scattered returns after beamforming and match filtering appears in Fig S5A, which is the same data as that presented in Fig 1G before conversion to fish population density. The lack of apparent speckle noise fluctuations in these images is a result of (i) our standard 6-sample intensity average, and (ii) inherent variance reduction from application of the matched filter to fluctuating signals received in an ocean waveguide (*S11*). The mean measured pressure level along the transect shown in Fig S5A appears in Fig S5B with experimentally determined standard deviations for our standard 6-sample (3-ping and 2-range-cell) intensity average. These measured standard deviations range from 1.1 to 1.6 dB as shown in Fig S5B or 29% to 45% of our standard 6-sample-averaged OAWRS intensity data. These measured standard deviations are consistent with the theory and previous measurements of received circular complex Gaussian field data (*S8*, *S12-S16*) after matched filtering and intensity averaging (*S11*). The expected two-way transmission loss (TL) along the Fig S5A transect is shown in Fig S5C, determined from parabolic equation based Monte Carlo modeling with measured bathymetry and oceanography. It is dominated by the two-way cylindrical spreading loss of a waveguide and has small variation over the depths where fish shoals were observed by CFFS (Fig 2). The mean two way TL trend is consistent with that of our measured pressure level in Figs S5B where large fish shoals are not found, i.e. ranges other than 9.5-13 km. Statistical analysis of our experimental data shows that the stationary averaging we employed leads to a standard deviation per pixel in the OAWRS population density estimates presented of roughly 1-2 dB in regions where shoal populations follow a stationary random process in space and time consistent with that determined by the simultaneous CFFS measurements needed to determine the expected fish scattering cross-section at OAWRS frequencies. This standard deviation is due to the combined effects of received field fluctuation from transmission, scattering, and source level calibration. We were not able to convert scattering strength to fish population density for the fish groups observed in regions shallower than the 100-m bathymetric contour due to lack of corresponding CFFS measurements of fish depth distributions and population densities in those regions. Fig 4A-D is left in terms of scattering strength because much of the population observed has migrated to depths shallower than 100 m.
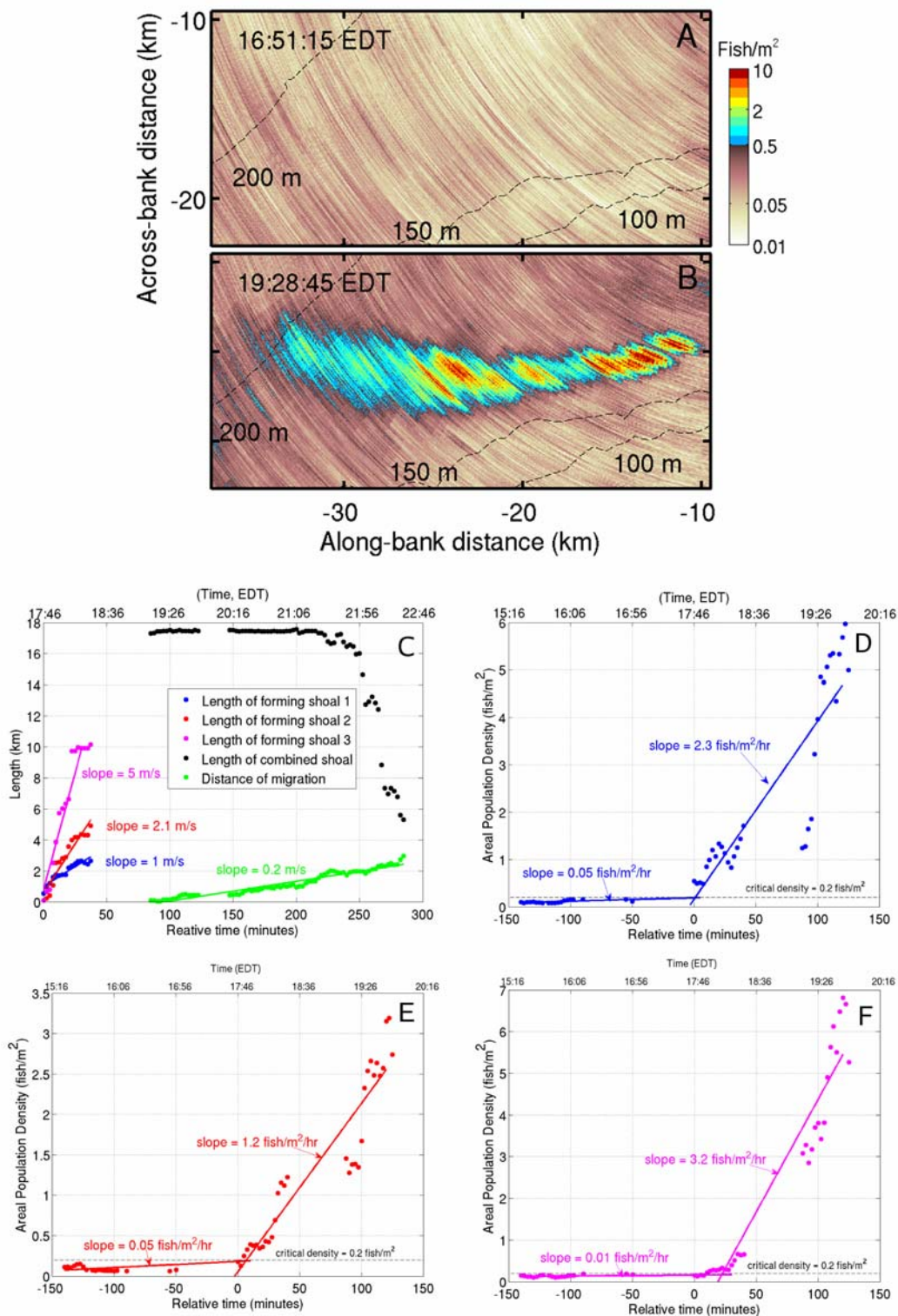
Fig S1. (A-B) OAWRS areal density (fish/m^2) on 2 Oct. 2006 illustrates shoal emergence near sunset, which was at 18:10 EDT. The origin of the coordinate system is at the source location 42.2089°N, 67.6892°W. Spatial location of region imaged is shown in Fig S6. (C) Shoal length (major axis) and migration distance versus time, including growth and migration speeds on the evening of Oct 2, 2006 from OAWRS imagery data. Shoal 1 (blue) initiates at (-12,-15), Shoal 2 (red) at (-27,-16) and Shoal 3 (magenta) at (-19,-16) in (along-bank, across-bank) coordinates of Fig S1A-B at 17:46 EDT. Magenta, red and blue solid lines are linear best fits for the data points, with slopes indicating shoal forming wave speeds. Shoals 1, 2 and 3 combine between 18:30 EDT and 19:00 EDT. Migration distance of combined shoal southern edge (green points) towards spawning area. Green solid line is linear best fit with slope indicating migration speed. (D-F) Mean areal population density versus time for Shoal 1 (blue data), 2 (red data) and 3 (magenta data) over respective 600 m x 600 m areas about their initiation coordinates from OAWRS imagery. Slow growth in population density before critical density is attained at 17:46 EDT. Immediately afterward density increases rapidly and shoal forming wave initiates.

3
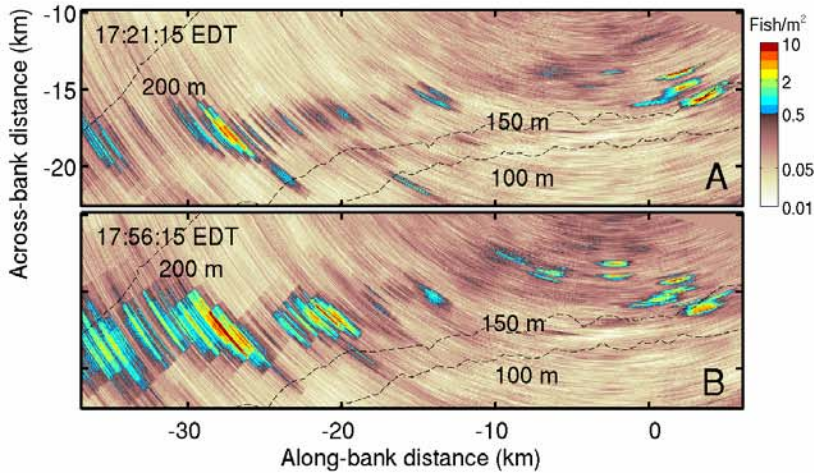
Fig S2. (A-B) OAWRS areal density (fish/m^2) on 1 Oct. 2006 illustrates sparse shoal emergence near sunset, which was at 18:11 EDT. The origin of the coordinate system is at the source location 42.2089°N, 67.6892°W. (C) Shoal length (major axis) and migration distance versus time, including growth and migration speeds on the evening of Oct. 1, 2006 from OAWRS imagery data. Shoal initiates at (2,-12) in (along-bank, across-bank) coordinates of Fig S2A-B at 15:33 EDT. Black solid line is linear best fit for the data points with slope indicating shoal forming wave speed. Migration distance of the shoal's southern edge (green points) towards spawning area. Green solid line is linear best fit with slope indicating migration speed. (D) Mean areal population density of the shoal versus time over a 600 m x 600 m area about its initiation coordinates from OAWRS imagery. Slow growth in population density before critical density is attained at 15:33 EDT. Immediately afterward density increases rapidly and shoal forming wave initiates.

4
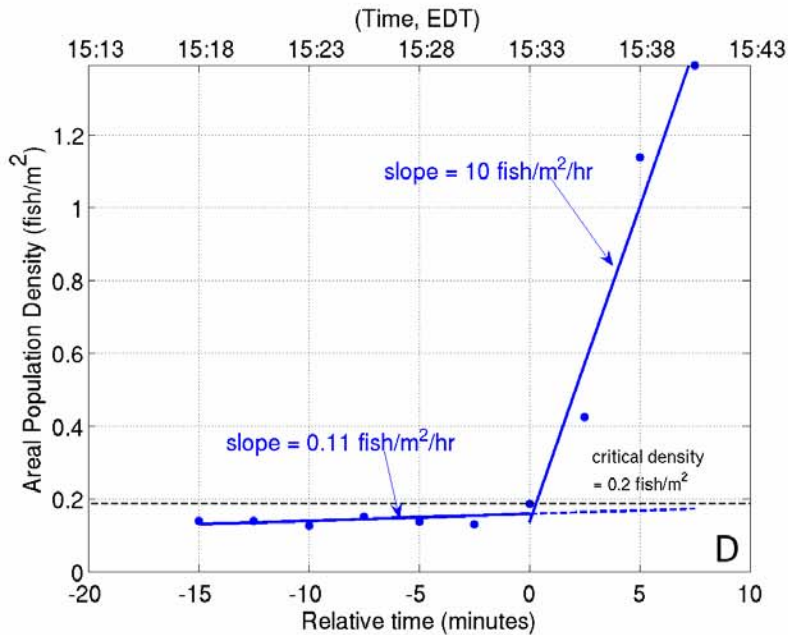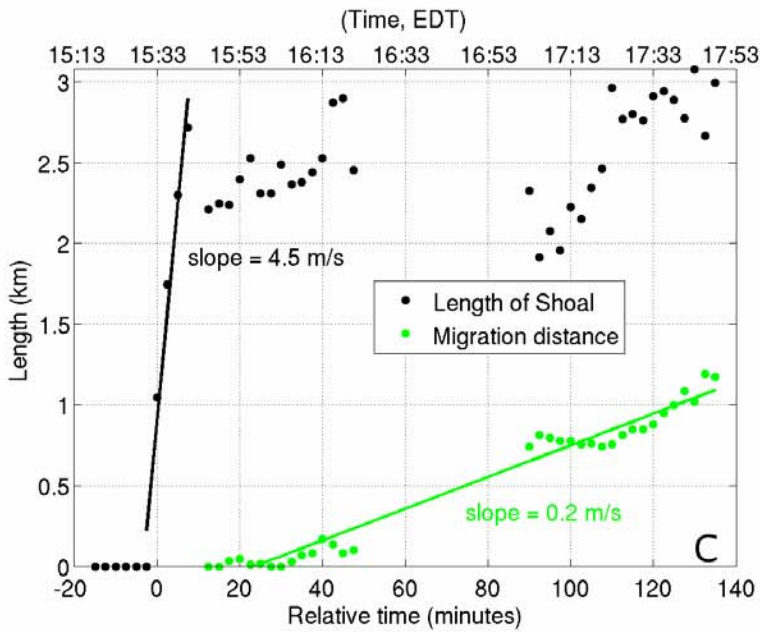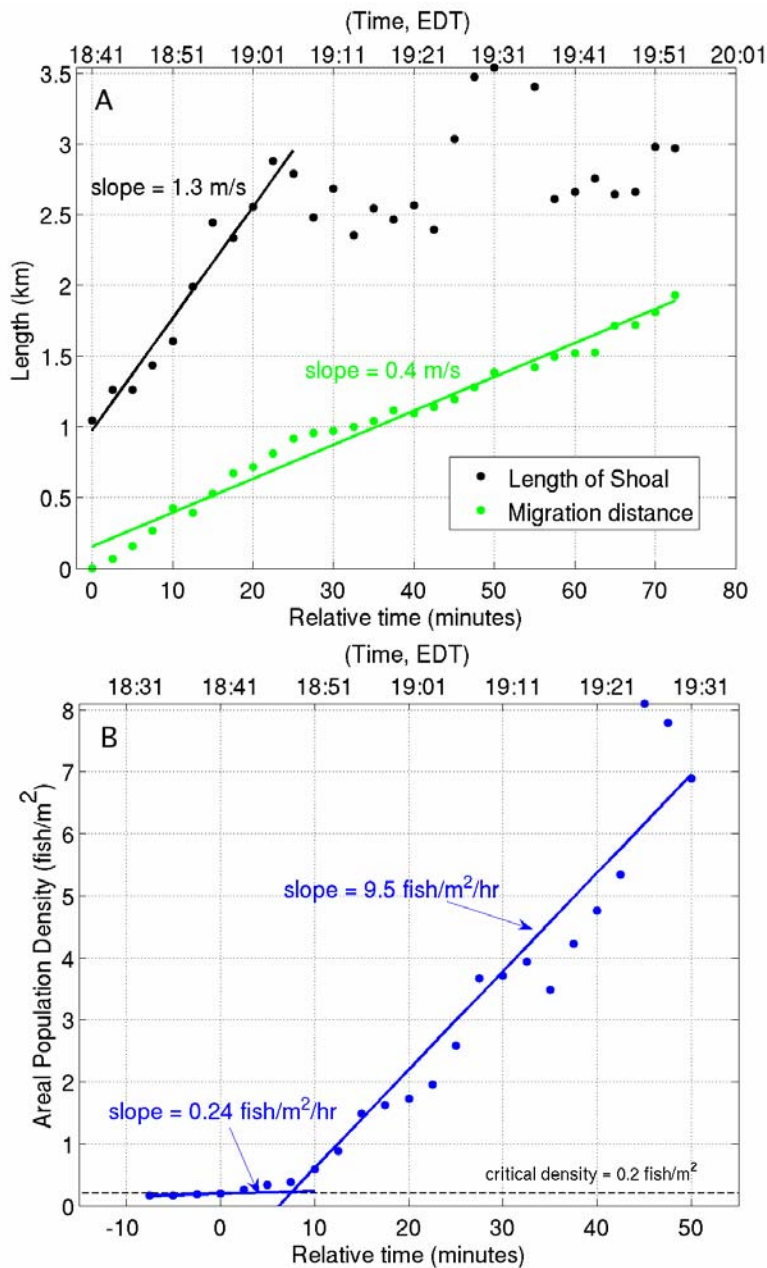
Fig S3. (A) Shoal length (major axis) and migration distance versus time, including growth and migration speeds on the evening of Sept. 29, 2006 from OAWRS imagery data. Shoal initiation was missed due to a data gap. An already initiated shoal of 1 km length passes through (5,-12) in (along-bank, across-bank) coordinates of Fig 4A-D at zero relative time and continues to grow. Black solid line is linear best fit for the data points with slope indicating shoal forming wave speed. Migration distance of the shoal's southern edge (green points) towards spawning area. Green solid line is linear best fit with slope indicating migration speed. (B) Mean areal population density of the shoal versus time over a 600 m x 600 m area about its southern edge. Slow growth in population density before critical density is attained at 18:51 EDT. Immediately afterward density increases rapidly as shoal forming wave propagates through.
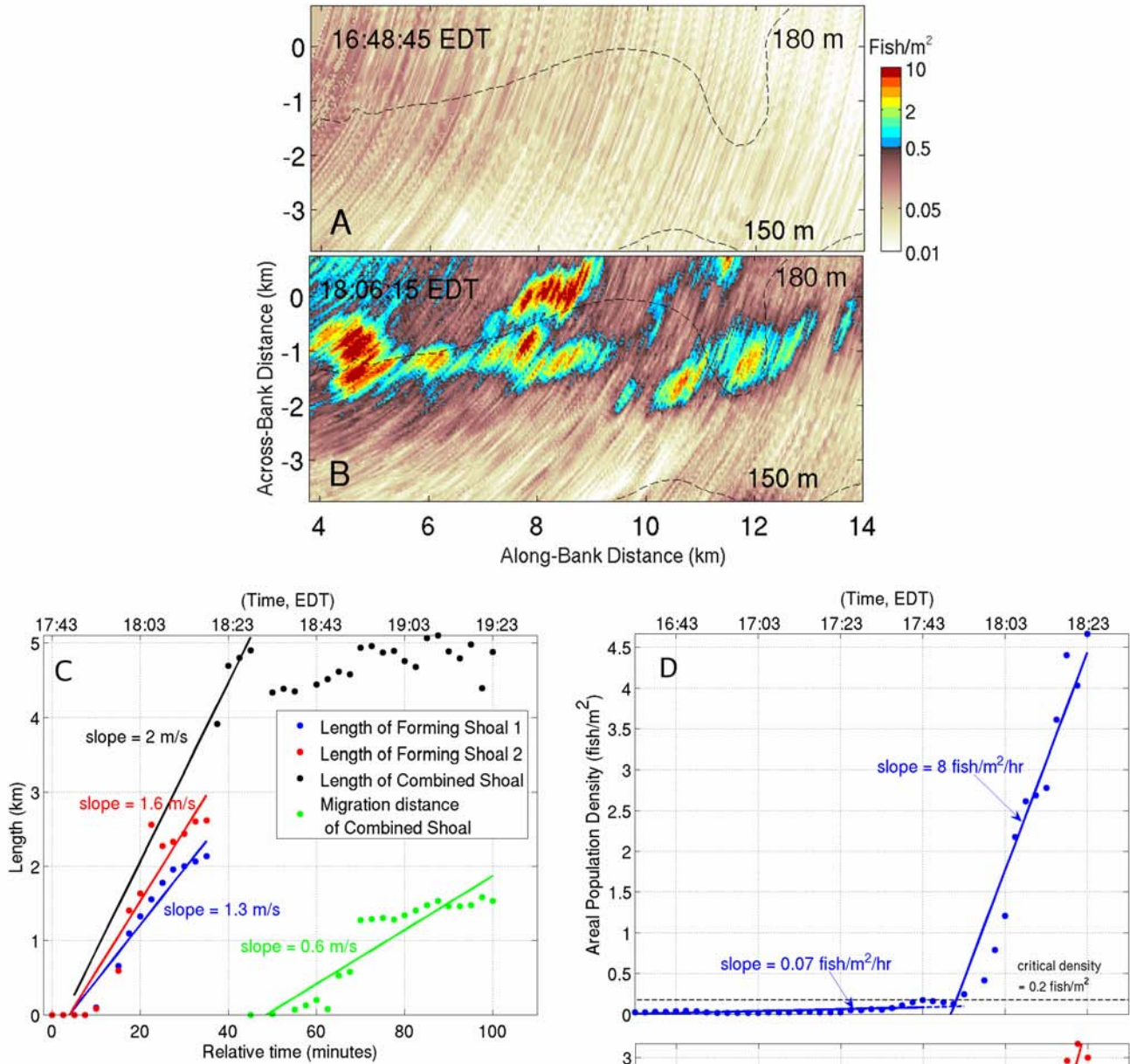
Fig S4. (A-B) OAWRS areal density (fish/m^2) on 28 Sept. 2006 illustrates shoal emergence near sunset, which was at 18:17 EDT. The origin of the coordinate system is at the source location 41.9397°N, 68.1°W. (C) Shoal length (major axis) and migration distance versus time, including growth and migration speeds on the evening of Sept. 28, 2006 from OAWRS imagery data. Shoal 1 (blue) initiates at (10.5,-2) and Shoal 2 (red) at (12,-1.5) in (along-bank, across-bank) coordinates of Fig S4A-B at 17:43 EDT. Red and blue solid lines are linear best fits for the data points, with slopes indicating shoal forming wave speeds. Shoals 1 and 2 combine at 18:19 EDT. Migration distance of combined shoal southern edge (green points) towards spawning area. Green solid line is linear best fit with slope indicating migration speed. (D-E) Mean areal population density versus time for Shoal 1 (blue data) and 2 (red data) over respective 600 m x 600 m areas about their initiation coordinates from OAWRS imagery. Slow growth in population density before critical density is attained at 17:43 EDT. Immediately afterward density increases rapidly and shoal forming wave initiates.
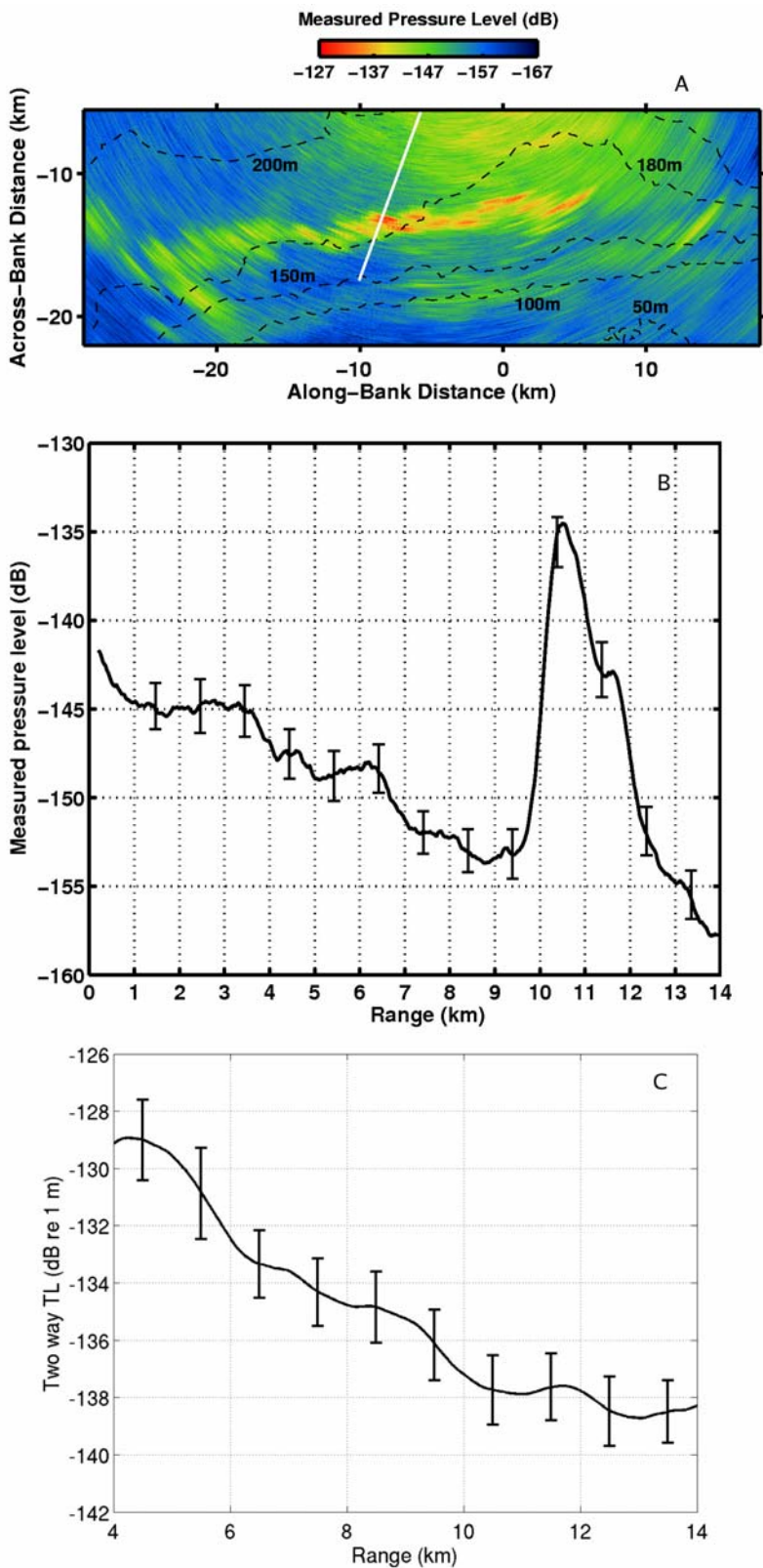
Fig S5. (A) Measured pressure level of scattered returns after beamforming and match filtering in dB re 1 m, normalized to unit source power. Same data as that presented in Fig 1G before conversion to fish population density, with our standard 6-sample (3-ping and 2-range-cell) intensity average. (B) Mean measured pressure level along the transect in Fig S5A appears with experimentally determined standard deviations for our standard 6-sample (3-ping and 2-range-cell) intensity average. (C) Expected two way transmission loss (TL) along transect in S5A for depth-averaged intensity within 40 m of the seafloor where fish shoals were observed by CFFS (Fig 2). Computed by parabolic equation-based Monte Carlo modeling (*S11*) with measured bathymetry and oceanography. The trend is dominated by two-way cylindrical spreading. Error bars show roughly 1 dB standard deviation of 40-m depth average at given ranges indicating low variation in expected 2-way TL over fish shoal depths observed in Fig 2.
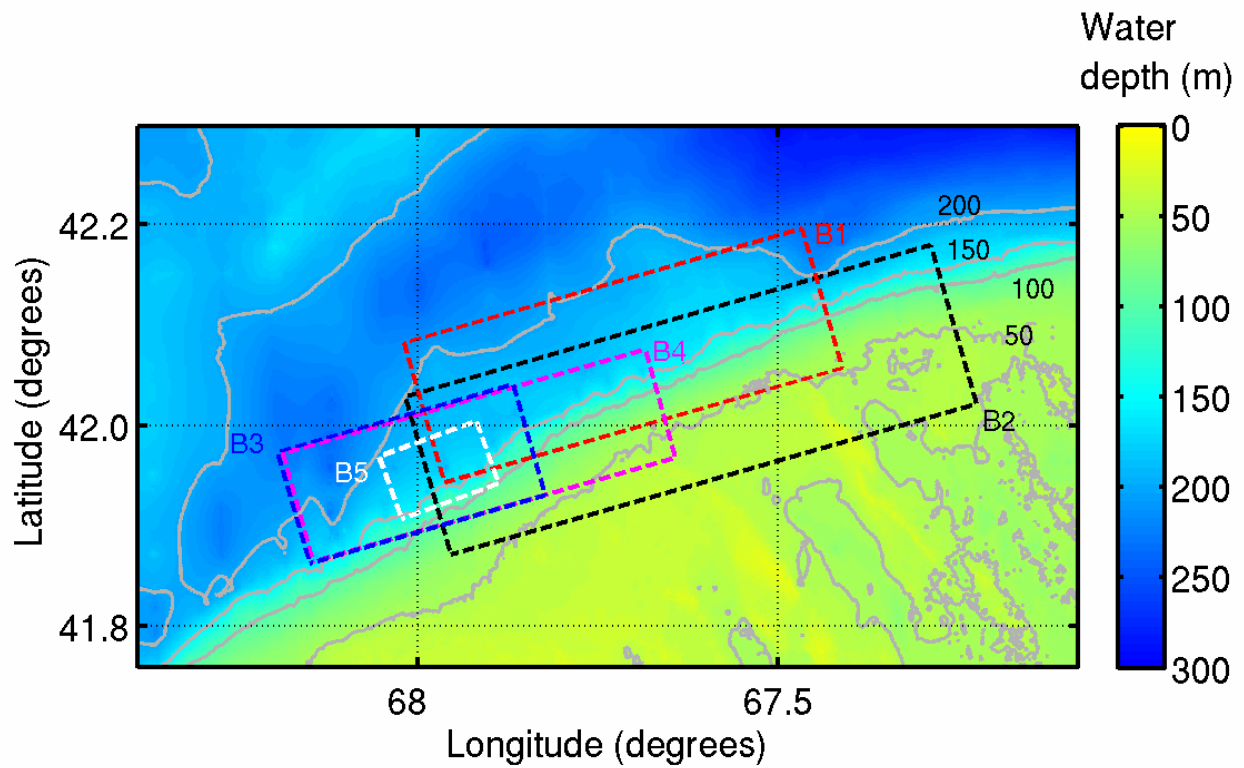
Fig S6. Georges Bank bathymetry in the region of the OAWRS images shown in Figs S1-S4. Boxes B1 and B2 are regions shown in Fig 1G-L and Fig 4A-D, respectively. Boxes B3, B4 and B5 are regions shown in Figs S1A-B, S2A-B and S4A-B respectively.

Supporting references and notes

S1.Lord Rayleigh, *The Theory of Sound* (Dover, New York, 1896), Vol. 2, Ch. 15, p. 296.

S2. J. Toner, Y. Tu, *Physical Review E.*, **59 (4)** (1998).

S3. D. V. Radakov, in *Schooling in the ecology of fish* (John Wiley & Sons, New York, 1973).

S4. P. Fréon, O. A. Misund, *Dynamics of Pelagic Fish Distribution and Behavior: Effects on Fisheries and Stock Assessment* (Fishing News Books, Oxford, 1999).

S5. O. A. Misund, A. Aglen, and E. Froenaes, *ICES J. Mar. Sci.*, **52 (1)** (1995).

S6. F. Gerlotto, M. Soria, P. Fréon, *Can. J. Fish. Aquat. Sci.* **56** (1999).

S7. T. J. Pitcher, in *Encyclopedia of Ocean Sciences*, J. H Steele, K. K. Turekian, S. A. Thorpe, Eds. (Academic Press, London, 2001), pp. 978-987.

S8. N. C. Makris, P. Ratilal, D. T. Symonds, S. Jagannathan, S. Lee, R. W. Nero, *Science*, **311**, 660-663 (2006) and Supporting Online Material.

S9. R. Urick, *Principles of Underwater Sound* (McGraw-Hill, New York, 1983).

S10. Chen, Ratilal, Makris, *J. Acoust. Soc. Am.* **118**, 3560 (2005).

S11. Andrews, Chen, Ratilal, *J. Acoust. Soc. Am.* **125**, 111 (2009).

S12. J. W. Goodman, Statistical Optics (Wiley, New York, 1985).

S13. N. C. Makris, *J. Acoust. Soc. Am.* **100**, 769 (1996).

S14. N. C. Makris, *Opt. Lett.* **20**, 2012 (1995).

S15. N. C. Makris, L. Avelino, R. Menis, *J. Acoust. Soc. Am.* **97**, 3547 (1995).

S16. P. Ratilal, Y. Lai, D. T. Symonds, L. A. Ruhlmann, J. R. Preston, E. K. Scheer, M. T. Garr, C. W. Holland, J. A. Goff, and N. C. Makris, *J. Acoust. Soc. Am.* **117**, 1977-1998 (2005).